The Journal of the Oceanological Society of Korea
Vol. 11, No. 1, p. 18~24, June 1976

A NUMERICAL EXPERIMENT ON TIDAL CURRENTS IN ASAN BAY

*Hui Soo Ahn** and *Suk Woo Lee***
*Geophisical Institute of Tokyo University
Korea Ocean Science & Engineering Corp.

ABSTRACT

The distribution of tidal currents in Asan Bay was simulated by a numerical experiment.

A homogeneous and single layer model with bottom stress taken into account was used. Althuogh the effective configuration of the bay differs significantly between the high tide and the low tide, its form is assumed to be fixed as a first approximation.

The advective term is particularly large because the tidal range of 810 cm is large compared to the depth and the changes of velocities occur abruptly.

The results of calculations agree fairly well with the observations. For example, the tidal range at Manhoriis amplified 15 cm higher and the phase lag is five minutes later than at the mouth of the bay. It also can generally be said that, with the semidiurnal tide at the mouth of the bay, the tidal range is increased toward the inner corner and that tidal currents are found to be large at the deeper part of the bay.

INTRODUCTION

In most cases of numerical computation for tidal waves travelling over the oceans, a linear model with bottom stress neglected and with the tide-generating potential given on the surface of the oceans has proved to be satisfactory (e.g. Ueno, 1963). However, in a small bay tidal velocities become large and abruptly change from place to place, so that the role of the non-linear term increases, while the effect of the coriolis term decreases and the bottom stress term can not be neglected because of the shallow depth.

Asan Bay, which is located at the central part of the west coast of Korea, has about 100 km^2 of area at flood tide and 50 km^2 at ebb tide. The average depth of the whole bay is five meters, its deepest part near the mouth of the bay being 20 meters.

Not many observations of tides in or around Asan Bay have been made, but recently the Korea Ocean Science & Engineering Corporation Lee, Suk Woo, Rep.) recorded tides at Nomi tidal station for two months and at Manhori tidal station for one month. The harmonic constants of the main four tidal components observed at Manhori and Nomi are shown in table 1.

In order to simulate the tidal current distribution of Asan Bay with a finite difference method, a grid spacing of 0.5 by 0.5 km was used.

Fig.1 shows the bay, the form of which is assumed to be fixed as indicated by the gothic line. We put the points of depth at the centers of the lattices, and calculate the model depth under the following considerations: first, the volume of the model is almost the same as that of the bay: second, for the sake of convenience

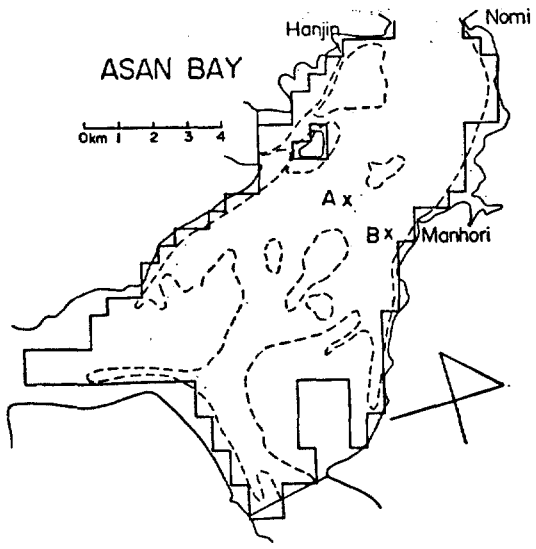

Fig. 1. Topography of Asan Bay. The thick line indicates the boundary of the model which is divided to meshes of 0.5 by 0.5 km. The dashed line shows the boundary of beach at ebb tide.

Table 1. The harmonic constants of the main four tidal components observed at Manhori and Nomi.

	Nomi (37°00′00″N, 126°46′52″E)		Manhori (36°57′40″N, 126°50′50″E)	
	H(cm)	K(°)	H(cm)	K(°)
M_2	290.6	127.6	299.5	131.6
S_2	115.0	175·7	116.8	178.8
K_1	37.0	306.0	38.5	305.6
O_1	28.4	259.8	27.2	262.2

of calculation, the depth will be taken one meter deeper than the datum level at the points in the beach at ebb tibe in order to keep them under water: third, the water transports flow only through the mouth of the bay and the runoff from the streams flowing into the bay is neglected.

The purpose of the present study is to calculate the distribution of tidal currents in the bay by means of the numerical experiment.

THE METHOD OF CALCULATION

A. Fundamental equations.

A homogeneous, non-linear and single layer model was used. The fundamental equations of the tides are as follows, Equations of motion,

$$\frac{du}{dt}-fv=-\frac{1}{\rho}\frac{\partial p}{\partial x}+Av\frac{\partial^2 u}{\partial z^2}+AlV_H^2u \quad (1)$$

$$\frac{dv}{dt}+fu=-\frac{1}{\rho}\frac{\partial o}{\partial y}+Av\frac{\partial^2 v}{\partial z^2}+AlV_H^2v \quad (2)$$

$$\frac{dw}{dt}=-\frac{1}{\rho}\frac{\partial p}{\partial z}+g. \quad (3)$$

Equation of continuity,

$$\frac{\partial u}{\partial x}+\frac{\partial v}{\partial y}+\frac{\partial w}{\partial z}=0. \quad (4)$$

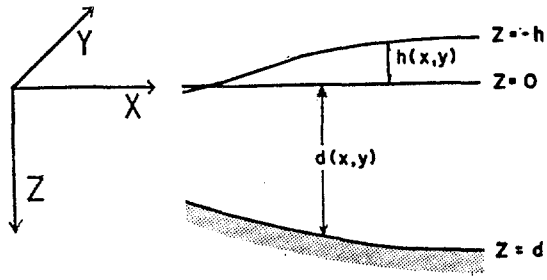

Fig. 2. The coordinate system.

We adopt the right handed coordinate system shown in Fig. 2, where the z coordinate is positive downward. The symbols of variables used in the above equations are;

u, v, w; velocity components in the x,y,z directions.

f; coriolis parameter, $f=2\Omega\sin\varphi$ where Ω is the angular velocity of the earth and φ is latitude.

ρ; density of sea water.

Av, Al; vertical and larteral turbulent viscosity coefficients.

p; pressure.

g; gravity acceleration.

V_H^2; horizontal Laplacian.

$$\frac{d}{dt}=\frac{\partial}{\partial t}+u\frac{\partial}{\partial x}+v\frac{\partial}{\partial y}+w\frac{\partial}{\partial z}.$$

If we neglect the acceleration of w in equation (3) (hydrostatic approximation), pressure can be expressed by using the elevation h from the mean sea level. Accordingly the pressure term in equations (1) and (2) is given as

$$-\frac{1}{\rho}Vp=-gVh.$$

If we integrate the equation (1), (2) and (4) from sea surface to bottom, the equations for the transport M and N are given by;

$$\frac{\partial M}{\partial t}=-g(d+h)\frac{\partial h}{\partial x}+T_s^x-T_B^x+fN$$
$$-(d+h)\left\{\frac{\partial u^2}{\partial x}+\frac{\partial uv}{\partial y}\right\}+AlV_H^2M \quad (5)$$

$$\frac{\partial N}{\partial t}=-g(d+h)\frac{\partial h}{\partial y}+T_s^y-T_B^y-fM$$
$$-(d+h)\left\{\frac{\partial uv}{\partial x}+\frac{\partial v^2}{\partial y}\right\}+AlV_H^2N \quad (6)$$

$$\frac{\partial h}{\partial t}=-\frac{\partial M}{\partial x}-\frac{\partial N}{\partial y}, \quad (7)$$

$(T_s^x,\ T_s^y)$ and $(T_B^x,\ T_B^y)$ are the $x-y$ components of the frictional stress at the surface and the bottom respectively. Here, we neglect the surface stress. On the other hand, bottom stress is taken into consideration by the following formula,

$\boldsymbol{T}_B=\rho\gamma_b^2\ V(\boldsymbol{V})$, here $\boldsymbol{T}_B=(T_B^x,\ T_B^y)$, $\boldsymbol{V}=(U,V)$

where the bottom frictional coefficient γ_b^2 is taken to be 0,0026.

B. Finite difference equation.

We transform the equations (5), (6) and (7) into finite difference equations by using the following transformation and putting $\Delta x=\Delta y=\Delta s$,

$$SX=M\frac{\Delta t}{\Delta s}=(d+h)u\frac{\Delta t}{\Delta s}$$

$$SY=N\frac{\Delta t}{\Delta s}=(d+h)v\frac{\Delta t}{\Delta s}.$$

We use the forward method for time dependent term and the centered method for space. The lattices of finite difference and the disposition of variables are indicated in Fig.3. The depth

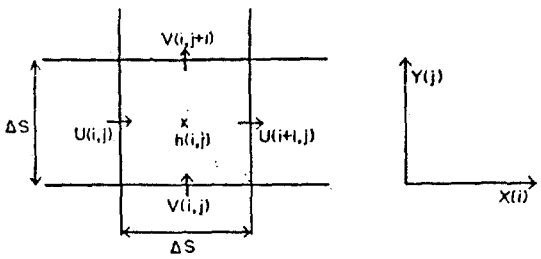

Fig. 3. The positions of variables of the meshes.

d and the elevation h are put at the centers of lattice squares and SX, u and SY, v are put in the mid points of the sides of the lattices squares. The finite difference equations of SX, SY and h are as follows,

The expression hx and by means the averages of two neighboring points of h as follows,

$$hx(i,j)=\frac{1}{2}(h(i,j)+h(i-1,j))$$

$$hy(i,j)=\frac{1}{2}(h(i,j)+h(i,j-1)).$$

This is same form. In equations (8), (9) and (10), the left hand terms are at time $t+1$ and the right hand terms are at time t. We calculate new values at $t+1$ from SX, SY, u and v at t.

Following equations of AX and AY are the finite difference analogues of the inertial term,

$$SX^{t+1}(i,j)=SX^t(i,j)-\frac{q}{2}\left(\frac{\Delta t}{\Delta s}\right)^2\{h^t(i,j)+h^t(i-1,j)+2dx(i,j)\}\cdot\{h^t(i,j)-h^t(i-1,j)\}-\gamma_2{}^b\left(\frac{\Delta t}{\Delta s}\right)^2$$
$$u^t(i,j)\sqrt{[u^t(i,j)^2+\{(v^t(i,j)+v^t(i-1,j)+v^t(i-1,\ j+1)+v^t(i,j+1))/4\}^2}+\frac{f\Delta t}{4}(SY^t$$
$$(i,j)+SY^t(i-1,j)+SY^t(i-1,j+1)+SY^t(i,j+1)]+\frac{(\Delta t)^2}{\Delta s}T_s^x+AX^t(i,j) \quad (8)$$

$$SY^{t+1}(i,j)=SY^t(i,j)-\frac{q}{2}\left(\frac{\Delta t}{\Delta s}\right)^2[h^t(i,j)+h^t(i,j-1)+2\mathrm{dy}(i,j))\cdot(h^t(i,j)-h^t(i,j-1)]-\gamma_2{}^b\frac{(\Delta t)^2}{\Delta s}$$
$$v^t(i,j)\sqrt{[\{u^t(i,j)+u^t(i+1,j)+u^t(i,j-1)+u^t(i+1,j-1))/4\}^2+(v^t)i,j)]^2}-\frac{f\Delta t}{4}(\mathrm{SX}^t$$
$$(i,j)+SX^t(i+1,j)+SX^t(i,j-1)+SX^t(i+1,j-1))+\frac{(\Delta t)^2}{\Delta s}T_s^y+AY^t(i,j) \quad (9)$$

$$h^{t+1}(i,j)=h^t(i,j)-SX^t(i+1,j)+SX^t(i,j)-SY^t(i,j+1)+SY^t(i,j) \quad (10)$$

$$AX(i,j)=\frac{1}{8}\left(\frac{\Delta t}{\Delta s}\right)^2(h(i,j)+h(i-1,j)+2dx(i,j))(u(i+1,j)-u(i-1,j))(u(i+1,j)+2u(i,j)+u(i-1,j))+(u(i,j+1)+u(i,j))(v(i,j+1)+v(i-1,j+1))-(u(i,j)+u(i,j-1))(v(i,\bar{e})+v(i-1,j))\} \quad (11)$$

$$AY(i,j)=\frac{1}{8}\left(\frac{\Delta t}{\Delta s}\right)^2(h(i,j)+h(i,j-1)+2dy(i,j))\{(u(i+1,j)+u(i+1,j-1))(v(i+1,j)+v(i,j))-(ui,j)+u(i,j-1))(v(i,j)+v(i-1,j))+(v(i,j+1)-v(i,j-1))(v(i,j+1)+2v(i,j)+v(i,j-1))\} \quad (12)$$

There is no horizontal mixing term in equations (9) and (10). The effect of horizontal mixing is included in the smoothing process. The equations of smoothing are as follows,

$$SX(i,j)=(1-4D)SX(i,j)+D\{SX(i+1,j)+SX(i,j+1)+SX(i-1,j)+SX(i,j-1))\} \quad (13)$$

$$SY(i,j)=(1-4D)SY(i,j)+D\{SY(i+1,j)+SY(i,j+1)+SY(i-1,j)+SY(i,j-1))\} \quad (14)$$

where D is a smoothing coefficient which is equal to $A1\Delta t/(\Delta s)^2$. Finally, the mean velocities u and v averaged from surface to bottom are given by.

$$u(i,j)=\frac{\Delta s}{\Delta t}SX(i,j)/\frac{1}{2}(h(i'j)+h(i-1,j+2dx(i,j)) \quad (15)$$

$$v(i,j)=\frac{\Delta s}{\Delta t}SY(i,j)\frac{1}{2}(h(i,j)+h(i,j-1)+2dy(i,j)) \quad (16)$$

In the above calculations, the following constants are used:

$f=8.364\times10^{-5}$ sec^{-1}

$\rho=1$ gr$\cdot$cm^{-3}

$A1=10^6$ cm$^2\cdot$sec^{-1}

$g=9.8\times10^2$cm$\cdot$sec^{-2}

C. Initial and boundary conditions.

At the initial step of the calculation, all variables *SX*, *SY*, *u*, *v*, etc. are set to zero.

On the boundary, the non-slip condition that the velocities parallel and perpendicular to the boundary are zero is satisfied, that is, $M=N=0$. The variables located on the shore line are all zero as shown in Fig. 4.

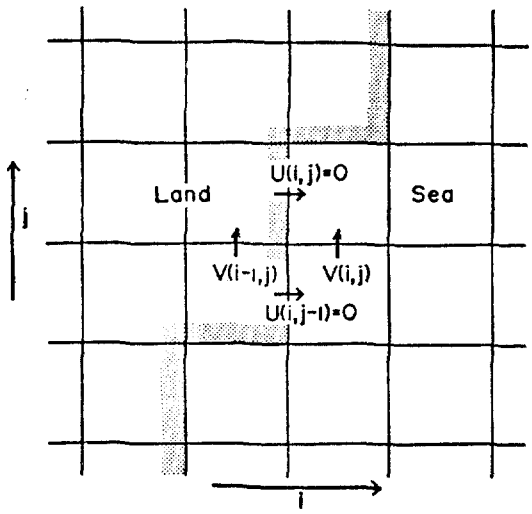

Fig. 4. The boundary condition. The variables on the boundary are zero. But the place of V(i-1,j) *which is just inside the boundary must be* changed into the negative value of V(i,j).

$SX(i,j)=u(i,j)=\cdots\cdots=0.$

Variables on the land($d=0$) are also zero. But the calculation of smoothing and non-linear terms needs the values of variables on the land which are not zero. That is, in Fig. 4, $SY(i-1,j)=-SY(i,j)$, $v(i-1,j)=-v(i,j)$, in order to satisfy the viscous boundary condition.

Here, it is important to decide the length of the time interval Δt compared to the space interval Δs. Among possible waves, the gravity wave is the fastest transmitting phenomenon in this case. So the condition of stability $\sqrt{3gH}\frac{\Delta t}{\Delta s}<1$ must be satisfied (e.g. Ueno, 1964) where H is the greatest depth. If we assume 20 meters for H and 0.5 km for Δs, then the time interval Δt must be less than 25 seconds. In the present computation we use 10 seconds for Δt.

The tidal problem in a small bay is treated

as a boundary value problem. The tidal record at Nomi station will be used as a boundary condition at the mouth of the bay because Nomi is very near the mouth of the bay. The characteristic feature of the tide observed at Nomi is nearly semi-diurnal $\left(\frac{Hl+Ho}{Hm+Hs}=0.16\right)$. So the tidal variation may be assumed to be a semi-diurnal sinusoidal curve with amplitude $(Hm+Hs)$ as a a first approximation, that is, the tidal elevation h is $h=405.0\sin\left(\frac{\pi}{6}T+t\right)$. Here, T is the lunar time and t is the starting time of the computation. One tidal period is approximated 12 hours.

D. The procedure of calculation.

According to the finite difference equations (8), (9), (10), (15) and (16), we can calculate SX, SY, u, v and h. But strictly speaking, the elevation h is computed at times 1/2 time step before SX and SY. The following diagram shows the procedure of calculation.

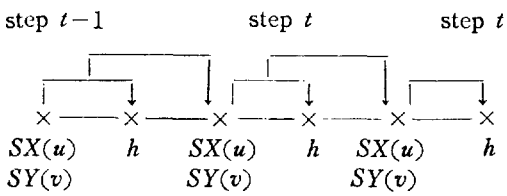

Although all terms of the equations of motion must be calculated in every time step, the terms except the local derivative and the pressure term are put into the calculation every five time steps because they have a small effect compared to these two terms and to calculate all terms in every time step consumes too much computer time. The calculation is allowed to proceed until it becomes stable.

RESULTS AND DISCUSSION

The time change of transport through the mouth of the bay is shown in Fig. 5. We can see that the calculation becomes stable after

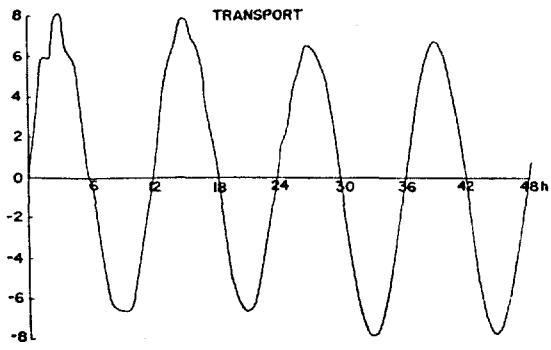

Fig. 5. The change of volume transport through the mouth of the bay. The units of vertical coordinate amount to 10^8 m^3.

three tidal periods since the curve of the third period almost resembles that of the fourth period.

Fig. 6 shows the distribution of tidal currents at the high, low and mid tides in the fourth period. The arrows indicates the vectors of tidal currents. The largest vector in the central part of the distribution diagram of 45 hours amounts to 318 cm/sec. The tidal currents at high and low tides are larger than at mid tides. As expected, the result shows that the larger velocities are in the deeper part of the bay.

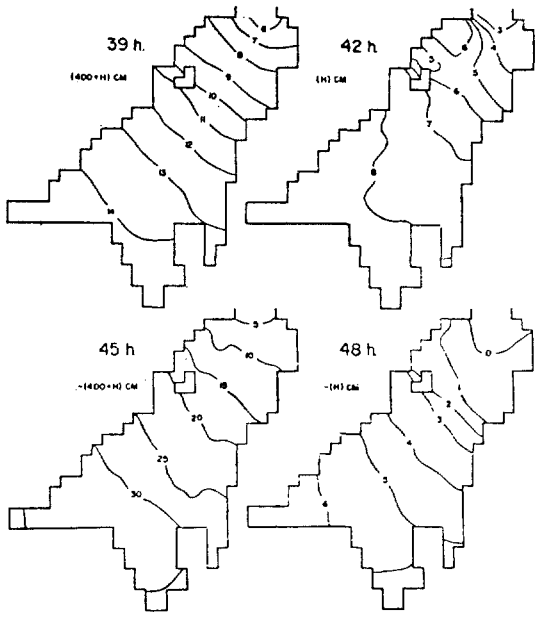

Fig. 7. Topography of the sea surface corresponding to fig.6.

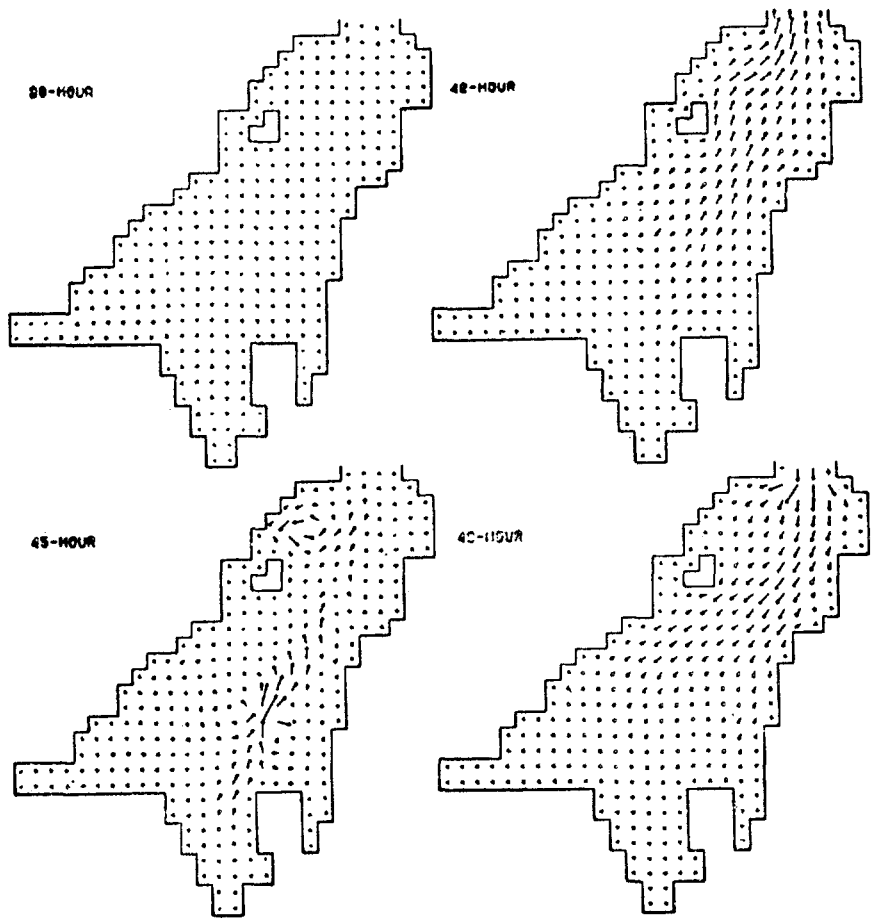

Fig. 6. The distribution of velocity vectors in fourth tidal period. The largest arrow in the figure of 45 hours amounts to 318 cm/sec.

But the extremely large values of velocities in the central and left upper parts of the 45 hour-diagram must be neglected, as they are outcomes of computational modes.

Fig. 7 is the contour diagram of the surface at the same time as fig. 6. We can easily see that the propagation of tides in the bay takes place as gravity waves because the contour lines are perpendicular to the axis of the bay. The phase lag which is attributed to the bottom topography is about 25 minutes between the mouth and the innermost corner.

Fig. 8 shows the tidal level variation at Manhori. The phase lag is five minutes and the tidal range is 825 cm which is amplified 15 cm higher than at the mouth of the bay. Although this amplified value is five centimeters smaller than the tidal range observed at Manhori tidal station, it agrees well with the observations considering the assumption that the tide at Nomi station, located outside of the bay, was used as a boundary condition at the mouth. The degree of amplification tends to increase toward the inner corner.

Fig. 9 shows the tidal current ellipses at two points A and B which are 1.5 km apart from each other between Manhori and Hyangdam island (cf. Fig. 1). The centers of ellipses

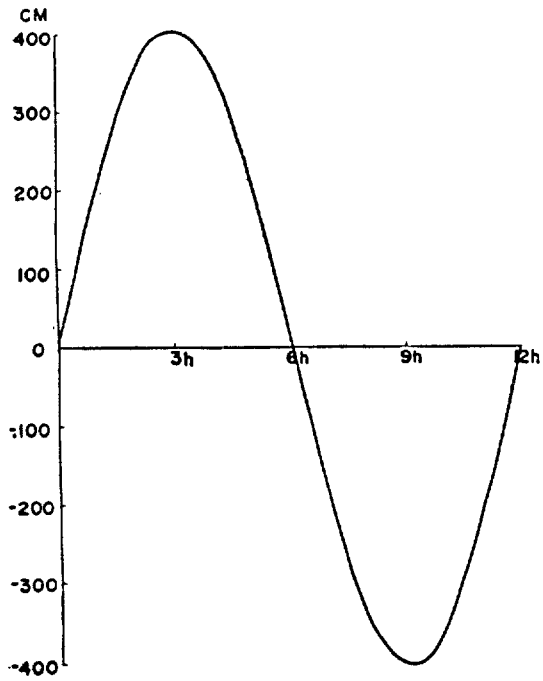

Fig. 8. The computed tital change at Manhori.

move -30cm/sec at point A and 20cm/sec at point B from each origin. This indicates a clockwise circulation in the bay. Generally the amount of tidal residual circulation is several percent of the tidal current in the ocean. It is uncertain whether this circulation is really the residual one or not because the order is very large compared to the tidal current. The calculation does not become stable yet so that the curves of the ellipses are not smooth. Comparing the results of the first, second, third and fourth periods, it can be said that it would become stable and the tendency would be the same if we continued for more times.

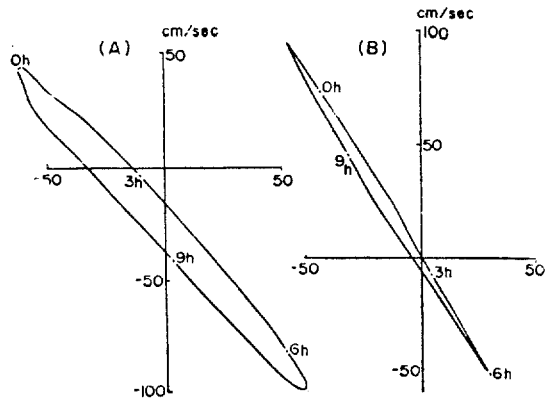

Fig. 9. The current ellipses at two points A and B.

ACKNOWLEDGEMENTS

The authors wish to express their thanks to Professor K. Yoshida for his encouragement and to Dr. N. Suginohara and others in Tokyo University for their advice and discussion.

REFERENCES

Ueno, T. 1963. Theoretical studies on tidal waves travelling over the rotating globe (1). Oceanogr. Mag., 15, 99-111.

Ueno, T. 1964. Non-linear numerical studies on tides and surges in the central part of Seto inland sea. Oceanogr. Mag., 16, 53-124.

Lee, S. 1974. Report on the Oceanographic Observation at Asan Harbor, Industrial Site and Water Resource Development Corp., M.O.C. 7-24.